High-performance bimetallic layer plasmonic sensors: a comparative study among Ti$_3$C$_2$T$_x$, black phosphorus and WS$_2$

Mohamed El Barghouti[1] · Abdellatif Akjouj[2] · Abdellah Mir[1]

Abstract

In this study, we explore by numerical computation a very sensitive biosensor with a high detection accuracy, a bimetallic rhodium (Rh)/gold (Au) nanostructure is proposed. A further improvement of the sensitivity and figure of merit (FoM) is obtained by applying a layer of LiNbO$_3$ and some 2D nanomaterials. Few nanolayers of Ti$_3$C$_2$T$_x$ MXene, black phosphorene (BP) and tungsten disulfide (WS$_2$) are selected to improve the detection performance of the nanoplasmonic biosensor. A detailed analysis was performed to design the high-performance biosensor by exploiting the optimization properties of each of the nanostructure layers for maximum sensitivity in the visible range at an excitation wavelength of 633 nm. The biosensor has a high sensitivity of 420 deg/RIU with a 228.125% improvement in sensitivity for analyte refractive indices ranging from 1.30 to 1.37 and FoM = 75.71 RIU^{-1}. The integration of Ti$_3$C$_2$T$_x$ MXene, BP or WS$_2$ with bimetallic in a conventional surface plasmon resonance biosensor offers a promising approach for bio- and chemical sensing, opening new possibilities for highly sensitive surface plasmon resonance biosensors using 2-dimensional nanomaterials.

Graphical Abstract
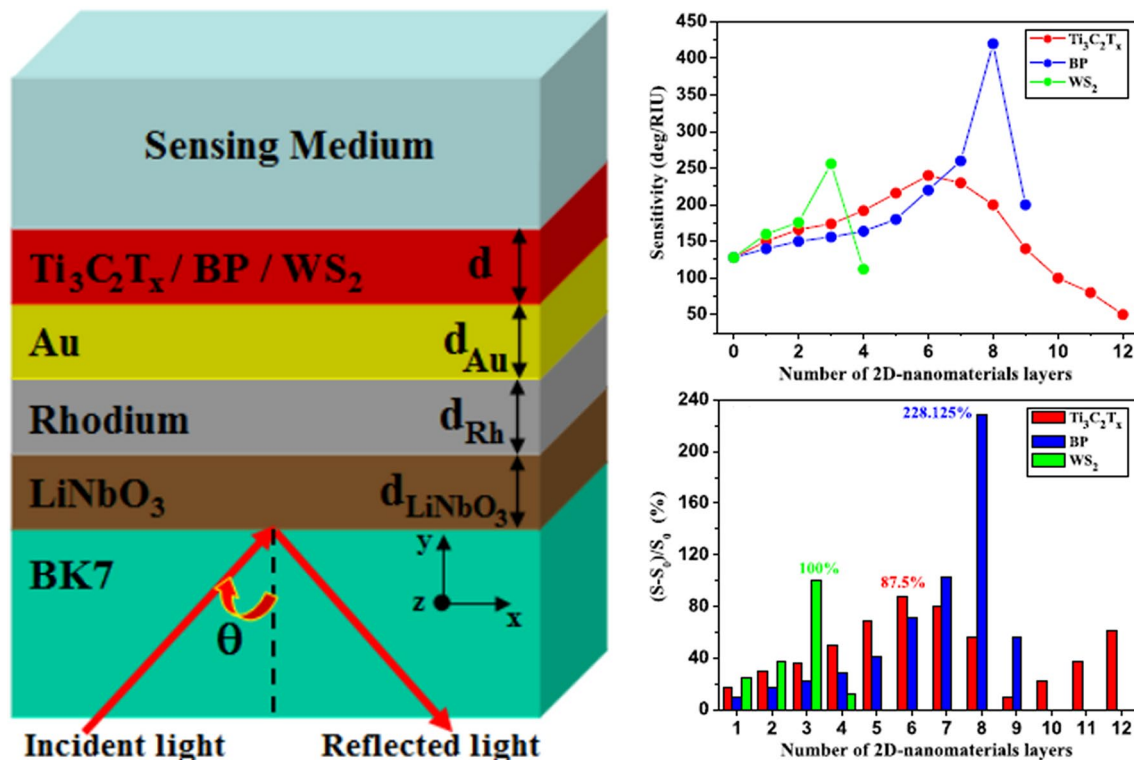
Extended author information available on the last page of the article

1 Introduction

Optical biosensors based on the electromagnetic response at the metal-dielectric interface has been called nanoplasmonics. Surface plasmonics (SPs) are free charge oscillations at the interface between a thin metal layer and a dielectric coating having a true dielectric permittivity of opposite signs. Surface nanoplasmonic resonance (SPR) has been widely used for biological and chemical detection in recent decades because of its superior performance, such as its ultrasensitivity, reliability, label-free and real-time detection capability [1–3]. According to the ATR (Attenuated Total Internal Reflection) coupler method, when the wave vector of the surface plasmons matches that of the incident transverse magnetic (TM) polarized excitation light, SPR occurs [4–6]. Plasmonic sensors are highly sensitive to changes in the refractive index (RI) of the detection medium. However, a small change in the refractive index of the analyte in the detection medium can result in an observable variation in the biosensor response or in the reflection intensity curve. When the resonance condition is satisfied, the incident TM polarized wave couples by resonance with the surface plasmons and a larger increase in the electric field strength causes a drop in the reflectance intensity curve.

Different types of SPR sensors, including prism-coupled SPR sensors [3], metallic-grating coupled SPR sensors [7], fiber-optic SPR sensors [8] and waveguide SPR sensors [9], have been designed and demonstrated for biochemical detection applications. The Kretschmann configuration [5] is a typical prism-coupled SPR sensor structure in which a thinner plasmonic metal film (e.g., Au, Ag, Al, ...) is deposited on the surface of a prism.

These metals have their own advantages and disadvantages such as Ag, although it is problematic for sulfidation with the environment, and is chemically unstable, Au does not form a thinner film [10, 11].

In the group of noble metals, a less often talked about metal is rhodium (Rh), a chemically inert element of the platinum group [12] which, due to its outstanding properties, is mainly used as a catalyst and in corrosion-resistant coatings. The large negative real part of Rh's permittivity is ideally suited for bio-detection based on nanoplasmonic resonance [13–16].

However, the metal layer must be stable against corrosion and oxidation, especially in the field of bio-sensing. As the different noble metals active for SPR such as Au, Al and Ag have different optoelectronic and chemical characteristics; it is difficult to select one of these metals with all the above ideal characteristics.

For example, Ag and Al give very fine plasmon resonance spectra, while Au has very stable optical and chemical characteristics. Various methods have been introduced to improve the performance of nanostructures in order to find an SPR biosensor with optimal characteristics. Meshginqalam et al. [17], Banerjee et al. [18] and Mishra et al. [13] have proposed a bimetallic structure containing a film of Ag or Al with an additional high index layer on the metallic film for electric field enhancement in the SPR structure.

In our proposed biosensor design, we were interested in a bimetallic Rh/Au nanoplasmonic structure. Due to the high imaginary part of the dielectric permittivity, the spectrum of Rh resonance is not very sharp, thus in conjugation with a very thin Rh film considered as Au film which dominates all noble metals in terms of sharpness of resonance and visibility. This bimetallic Rh/Au layer has the high sensitivity of Rh and the strong resonance of Au; however, the Au film, being the topmost layer, has the characteristic of chemical stability with the environment.

Two-dimensional (2D) nanomaterials, such as $Ti_3C_2T_x$ MXene [19, 20], transition metal dichalcogenides (TMDC) [21] and black phosphorus (BP) [22] have attracted considerable interest in recent years due to their unique optical, electrical and chemical outstanding characteristics and the application of these 2D nanomaterials in biosensors have been widely used to improve detection performance characteristics [23–28].

An SPR biosensor using $Ti_3C_2T_x$ MXene was designed in 2018 by Wu et al. to improve the sensor and the highest sensitivity is reported at 160 deg/RIU, which is covered by a four layer $Ti_3C_2T_x$ MXene [29]. In 2017, L. Wu et al. used a thin layer of BP and the highest sensitivity is reported at 181 deg/RIU [30]. An SPR biosensor using TMDC was designed by Zhao et al. to improve sensitivity and the highest sensitivity is reported at 237 deg/RIU which is covered by a WS_2 monolayer [31].

The main objective of all the designers of SPR bio- and chemical sensors is to obtain a better resolution and highest detection sensitivity.

In this study, we theoretically designed different SPR nanostructures by combining $Ti_3C_2T_x$, BP or WS_2 on a bimetallic Rh/Au nanostructure coupled by $BK7/LiNbO_3$ [BK7/$LiNbO_3$/Rh/ Au/($Ti_3C_2T_x$ or BP or WS_2)/sensing medium] as shown in Fig. 1. We can justify by saying that our proposed SPR biosensor based on the hybrid nanostructure has unique optical properties, such as the nanostructure is specially designed to improve the sensitivity and decrease the width at half maximum (FWHM), thus improving the performance of the biosensor compared to other conventional sensors. We

Fig. 1 Schematic illustration of the proposed bimetallic SPR biosensor nanostructure based on LiNbO$_3$ with the layer of nanomaterials; Ti$_3$C$_2$T$_x$ MXene, black phosphorene and WS$_2$
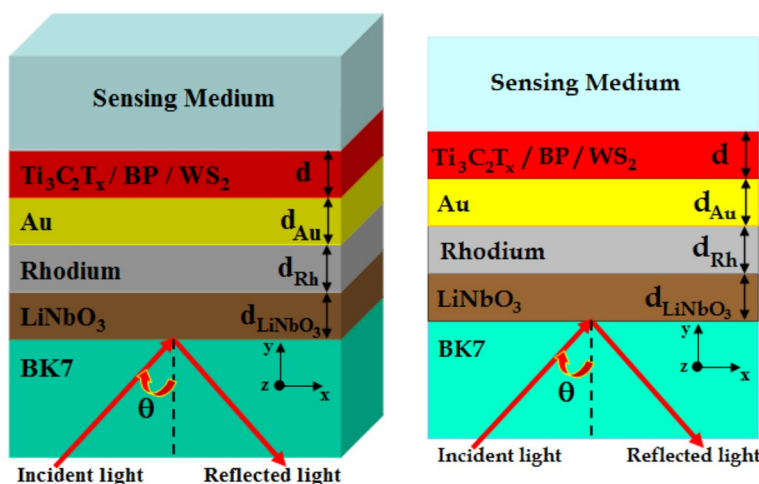
have achieved a significant improvement in angular sensitivity of 228.125%. Contrary to the traditional refractometer for example, our SPR biosensor can measure very small index variations between two biological liquids with very close index. It should be noted that the optimized sensitivity is 420 deg/RIU for eight layers of BP, 256 deg/RIU for three layers of WS$_2$, and times higher than the recently reported value of 240 deg/RIU for six layers of Ti$_3$C$_2$T$_x$.

2 Design consideration and theoretical model

2.1 SPR nanostructure overview

The proposed SPR biosensor nanostructure as shown in Fig. 1 is based on Kretschmann configuration. In this biosensor, we have taken a BK7 prism and LiNbO$_3$ layer is deposited on the base of prism of 10 nm thickness. Our SPR biosensor nanostructure based on the Rh/Au/2D material layers/sensing medium is shown in Fig. 1, which consists of six different layers. In this biosensor nanostructure, Rh as the noble metal for exciting SPs which is covered by a thin Au film is deposited on the BK7/LiNbO$_3$ as the coupling prism. Different 2D materials layer of Ti$_3$C$_2$T$_x$ MXene, BP and WS$_2$ are deposited between the Au film individually, and the last sensing medium is the biomolecular analyte as shown in Fig. 1.

A TM light from a monochromatic source at 633 nm wavelength is launched in one side of the BK7 prism, and reflected light is detected from the other side. When an electron or light beam is totally reflected at boundary, it generates an evanescent wave that interacts with the plasma wave if metal has appropriate thickness of tens of nanometers.

In this paper, we have designed different configurations using Ti$_3$C$_2$T$_x$ MXene, BP and WS$_2$ separately to optimize the performances parameters. Prism of lower refractive index offers high sensitivity [32], and therefore, we have considered a prism made of BK7 glass. The refractive index of BK7 glass has been calculated by using the following relation [33]:

$$n_{BK7} = \left(\frac{1.03961212\lambda^2}{\lambda^2 - 0.00600069867} + \frac{0.231792344\lambda^2}{\lambda^2 - 0.0200179144} + \frac{1.01046945\lambda^2}{\lambda^2 - 103.560653} + 1 \right)^{1/2}$$

(1)

where λ is the wavelength of incident light.

We have taken advantage of the fact that the design of the SPR biosensors implies the deposition of metallic films on the top side of the substrate, leaving the back side available for light injection in a classical Kretschmann prism-based SPR configuration.

The SPR nanostructures were fabricated on a glass substrate and LiNbO$_3$ is deposited on a prism base. LiNbO$_3$ was chosen for its excellent optical properties in the visible and near infrared for performance enhancement. In a simple approximation, the corresponding refractive indices can be calculated from a one-term Sellmeier equation [34, 35]:

$$n_{LiNbO_3} = \left[1 - \frac{A_0}{\lambda_0^2 / \lambda^2} \right]^{1/2}$$

(2)

With an average oscillator position λ_0 and a parameter A_0, which is a measure of the average oscillator strength at 633 nm, n$_{LiNbO_3}$ = 2.2864.

In order to describe the optical properties of metallic rhodium (Rh), the complex permittivity of the rhodium at the 633 nm is n$_{Rh}$ = $\sqrt{\varepsilon_{Rh}}$ = 2.152+i5.6102 [36].

The refractive index of Au film can be expressed from the Drude–Lorentz model [37]:

$$n_{Au} = \sqrt{\varepsilon_{Au}} = \left[1 - \frac{\lambda^2 \lambda_c}{\lambda_p^2(\lambda_c + i\lambda)}\right]^{1/2} \qquad (3)$$

where λ_p and λ_c represent the plasma and collision wavelength. The numerical values of λ_p and λ_c for gold (Au) are 1.6826×10^{-7}m and 8.9342×10^{-6}m, respectively.

The complex refractive index of $Ti_3C_2T_x$ MXene is considered as $n_{Ti_3C_2T_x} = 2.38 + i1.33$ and its thickness is varied as $d_{Ti_3C_2T_x} = L \times 0.993$ nm, where L is the number of $Ti_3C_2T_x$ MXene layers [38, 39]. As well, the complex refractive index of BP at the wavelength of 633 nm is reposted as $n_{BP} = 3.5 + i0.01$, and its thickness varied as $d_{BP} = M \times 0.54$ nm, where M is the number of BP layers [30]. The complex refractive index of WS_2 is considered as $n_{WS_2} = 4.9 + i0.3124$, and its thickness is varied as $d_{WS_2} = N \times 0.80$ nm, where N is the number of WS_2 layers [30]. Finally, the last layer is a sensing medium, and the refractive index is given as $n_s = 1.33 + \Delta n_s$, where Δn_s is the change of refractive index alteration due to bimolecular or biochemical change in the medium [40]. We will change this refractive index in our proposed SPR biosensor experiment, by the SPR-based binding method that involves the immobilization of a nanomaterial layer (ligand) on the biosensor surface, covalently attached to a gold surface. The layer of interest is immobilized on the sensor surface allowing solutions with different concentrations of an analyte to flow over it and characterize its interactions with the contact layer with the sensing medium (Fig. 1). The SPR signal comes from changes in the refractive index of the biosensor sensing medium. The increase in mass associated with a binding event causes a proportional increase in refractive index, which is observed as a change in SPR response. These changes are measured as changes in the resonance angle ($\Delta\theta_{SPR}$) of refracted light as the analyte, flowing through a microfluidic channel, binds to the layer at the sensing surface and increases in density at the biosensor sensing medium.

2.2 Theory and numerical methodology

The plasmonic spectral response has been evaluated by numerical calculations that are involved to study the optical properties SPR nanostructures using the Finite Element Method (FEM) based on COMSOL Multiphysics software [41, 42]. It contains in solving Maxwell's equations in the frequency domain by discretizing space into small finite elements (having different possible shapes). The Maxwell's equations in a region without source are given as:

$$\nabla \times \mathbf{E} = -\mu \frac{\partial \mathbf{H}}{\partial t} \qquad (4)$$

$$\nabla \times \mathbf{H} = \varepsilon \frac{\partial \mathbf{E}}{\partial t} \qquad (5)$$

where $\mathbf{E}$ and $\mathbf{H}$ are the electric and magnetic fields, respectively. ε is the permittivity, and μ is the permeability of the medium. In FEM method, Maxwell's equations are quantized according to the time and space. Solution of Maxwell's equations means evaluating the electromagnetic field's quantities in each space-time point according to the material parameters and initial conditions.

Assuming time-harmonic electric field, the electric field distribution in plasmonics nanostructures can be calculated by using the 2D vector wave equation:

$$\nabla \times \mu_r^{-1}(\nabla \times \mathbf{E}) - k_0^2 \varepsilon_r \mathbf{E} = \mathbf{0} \qquad (6)$$

where $\varepsilon_r(\omega) = \varepsilon_r'(\omega) - i\varepsilon_r''(\omega)$ is the complex dielectric function and ε_r', ε_r'' are its real and imaginary parts and $i = \sqrt{-1}$. $k_0 = \frac{\omega}{c}$ is the wave number in vacuum, and the relative permeability $\mu_r = 1$.

The SPR nanostructures are excited by an incident electromagnetic wave of wavelength $\lambda = 633$ nm and is generated in the substrate of refractive index n_{BK7}. It is launched in the Oxy plane with a varied angle of incidence (θ) relative to the Oy axis. This excitation wave is polarized TM, and its associated electric field vibrates along x and y-axes.

In the attenuated total reflection (ATR) configurations, the intensity reflectance coefficient (R) spectra can be calculated by using obtained S-parameters from numerical simulation as $R(\omega) = |S_{11}|^2$.

2.3 Performance parameters

In this study, we will present the different design principles of highly improved and highly sensitive SPR biosensors for biosensing applications. In order to compare detection performance, several major factors such as sensitivity (S), factor of merit (FoM) and field intensity enhancement will be introduced. The angle of incidence corresponding to the minimum reflectance intensity is called the plasmon resonance angle, and the detection angle sensitivity is calculated by the ratio between the spectral shifts of the plasmon resonance angle $\Delta\theta_{SPR}$ in degree and the variation of the refractive index of the detection medium Δn_s in RIU (Refractive Index Units) as follows [43]:

$$S = \frac{\Delta\theta_{SPR}}{\Delta n_s}(deg/RIU) \qquad (7)$$

Therefore, the sensitivity measurement is not sufficient to evaluate the performance of the biosensor. Thus, the other parameter needed to evaluate SPR biosensing performance is the Factor of Merit (FoM). The FoM is considered a useful parameter for verifying the SPR resolution. It is defined as the ratio of the refractive index sensitivity to the full width at half resonance height (Full Width at Half Maximum (FWHM)) [44]:

$$FoM = \frac{S}{FWHM}(RIU^{-1}) \qquad (8)$$

3 Results and discussion

In order to obtain optimized thicknesses of the constituent layers of the nanostructure for the SPR biosensor, we start by optimizing the thickness of the Rhodium layer. As for the different plasmonic nanostructures, the plasmonic response of Rhodium is strongly dependent on the thickness of their layer. By observing in Fig. 2 the SPR response, obtained by numerical computation, for the plasmonic nanostructure BK7/Rh/Sensing medium with variable layer thickness Rh only (d_{Rh}). We found that for d_{Rh}=10 nm Fig. 2a, the SPR reflectance curve has the best modulation depth (depth of the minimum in a spectrum of the SPR reflectance intensity).

In Fig. 2b, we show the SPR resonance angle of incidence (θ_{SPR}) as a function of d_{Rh} for two detection media n_s=1.33 and 1.37, we plot an improving SPR response with respect to the increase in d_{Rh}. On the same figure, we determine the sensitivity for the proposed structure and we find a better sensitivity of 145 deg/RIU at d_{Rh}=30 nm. For this thickness, the SPR curves show less modulation depth, FoM=6 RIU^{-1} low. Therefore, we choose d_{Rh}=10 nm. For this thickness, the minimum SPR reflectance intensity curve is zero (R_{min} =0) with the FWHM detection accuracy important, which gives a sensitivity of 56.25 deg/RIU and FoM=7.9 RIU^{-1} as the optimized thickness of the Rh layer for our further calculations.

It is shown that the high real part of Rh's permittivity leads to a higher sensitivity in plasmonic biosensors, while the high value of the imaginary part of their permittivity leads to a high loss of material which constitutes a measurement obstacle and limits the application of Rh in the field of detection. We have proposed an SPR nanostructure with a bimetallic Rh/Au layer is an appropriate approach to protect Rh loss and improve the performance of SPR biosensors.

An analytical study is performed to determine the optimal design to improve SPR performance. The bimetallic structure used with an Au layer above the Rh layer as a protective layer is shown in Fig. 3a. Figure 3b shows the variation of reflectance intensity versus angle of incidence for different thicknesses of the Au (d_{Au}) film at d_{Rh}=10 nm fixed. From Fig. 3, we notice that the reflectivity corresponding to the SPR resonance angle gradually increases with increasing Au film thickness from d_{Au}=3 nm to d_{Au}=30 nm due to increasing absorption. Figure 3c shows the variation of the minimum reflectance value (Rmin) at SPR as a function of the corresponding d_{Au} of two detection medium n_s=1.33 and 1.37. The minimum reflectance intensity (R_{min}) is obtained when the total energy transfers from the incident light to the plasmon resonance. In Fig. 3d, the biosensor sensitivity has been plotted against the Au film thickness for the structure with 10 nm Rh. It can be observed that the sensitivity is maximum 265 deg/RIU for an Au thickness of 30 nm.

It can be seen that the minimum reflectivity corresponding to the plasmon resonance angle is lower at the Au thickness of 20 nm which corresponds to a sensitivity of 125 deg/RIU. We consider this thickness as the optimized Au film thickness for the following calculations.

Unfortunately, the peak resolution of the conventional Rh-based (monometallic) SPR nanostructure is low and limits the FoM values, whereas a higher sensitivity is obtained. To overcome the low FoM value and the stability of the Rh-based SPR biosensor, we have studied the effect of Au in a modified bimetallic nanostructure with improved sensitivity (see Fig. 3).

In this research, we have calculated the FoM versus Au thickness with d_{Rh}=10 nm. As seen in Table 1, the FoM increases from 9.43 RIU^{-1} for d_{Au}=3 nm to 75.71 RIU^{-1}
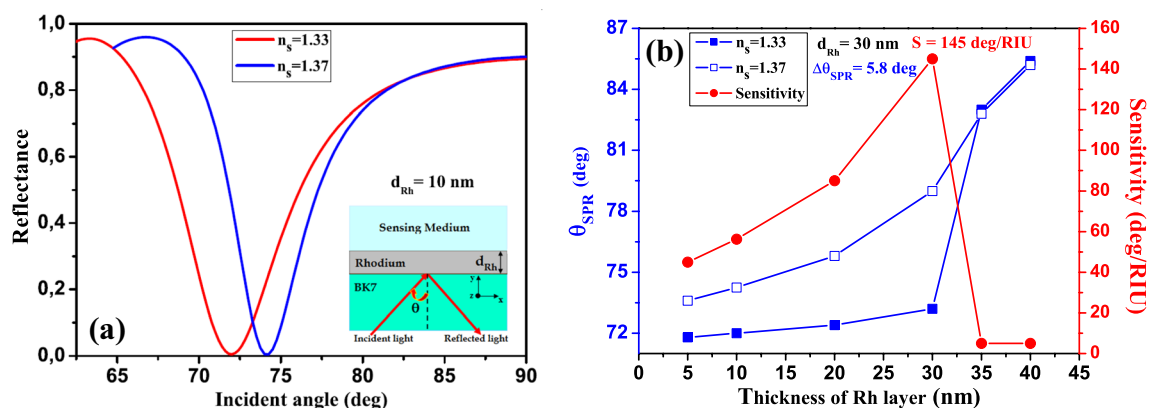

Fig. 2 **a** Reflectance intensity as a function of the incident angle for the variation of analyte refractive index n_s=1.33 (read line) and n_s=1.37 (blue line) for d_{Rh}=10 nm, **b** Evolution of the resonance angle (blue curves) and sensitivity (read curves) with thickness of Rhodium layer (d_{Rh})
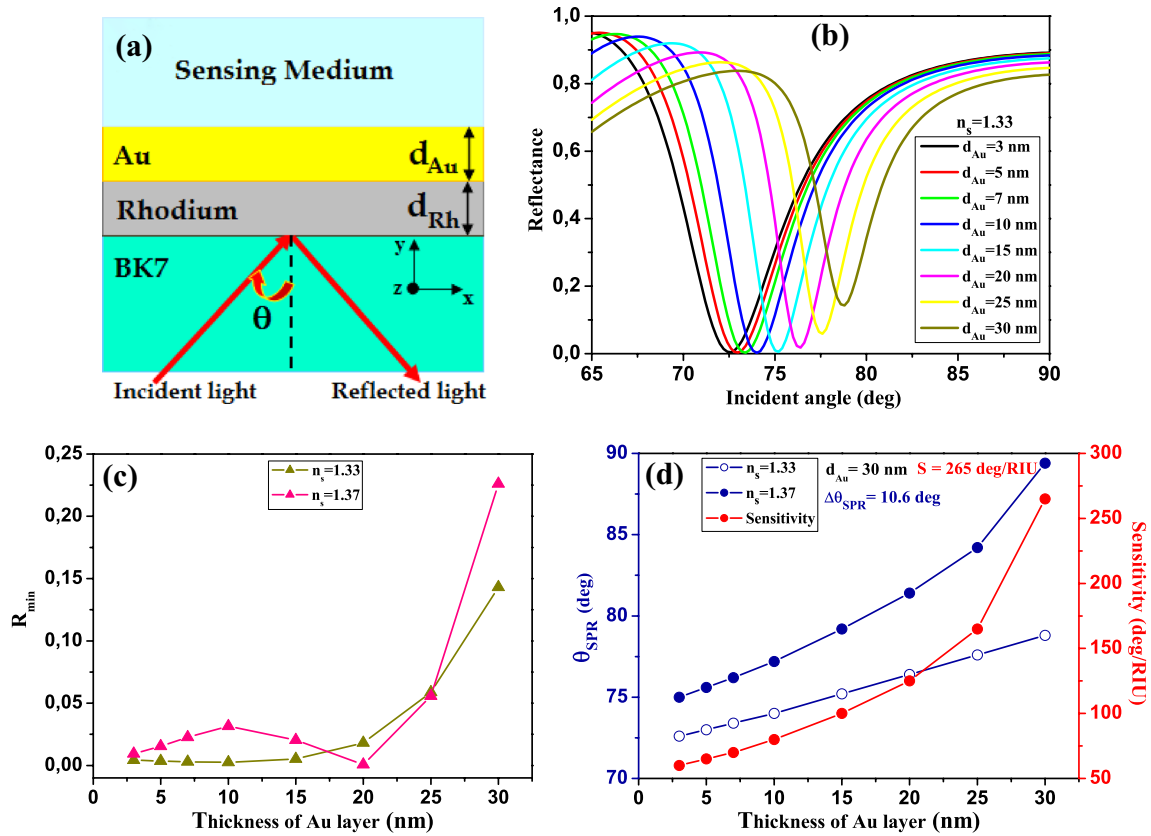
Fig. 3 a Schematic diagram of the designed bimetallic plasmonic nanostructure; **b** Reflectance intensity as a function of the incident angle and for different thicknesses of Au film (d_{Au}) with d_{Au}=10 nm; **c** Minimum reflectance values as a function of Au thickness for various analyte refractive index and **d** evolution of the resonance angle and sensitivity with thickness of Au film

Table 1 Performance comparison the nanostructure BK7/Rh(10nm)/Au/sensing medium for different thicknesses of Au film (d_{Au})

Thicknesses of Au film (nm)	Sensitivity (deg/RIU)	FWHM (deg)	FoM (RIU^{-1})
3	60	6.36	9.43
5	65	5.9	11
7	70	5.51	12.7
10	80	4.97	16.01
15	100	4.27	23.42
20	125	3.57	35.01
25	165	3.5	47.14
30	265	3.5	75.71

for d_{Au}=30 nm, which is greater than FoM=7.9 RIU^{-1} obtained with the BK7/Rh(10 nm)/sensing medium nanostructure. This gives an improved FoM of 858.35% (9.58 times) calculated for the bimetallic nanostructure compared to the monometallic nanostructure. This nanostructure is chosen as the best SPR configuration for real-world biosensing applications.

In this study, we present a biosensor for the detection of bimetallic surface plasmon resonance. Generally, SPR sensors are manufactured on non-piezo-active glass substrates; therefore, we studied the effect of a piezoelectric material LiNbO$_3$ [45, 46].

Figure 4 shows the SPR results of the structure on a piezoelectric substrate (BK7/LiNbO$_3$/ Rh(10 nm)/Au(20 nm)/sensing medium). As is clearly shown in Fig. 4a, the curves of reflectance intensity versus angle of incidence of light of wavelength 633 nm for different thicknesses of the LiNbO$_3$ layer (d_{LiNbO_3}). As expected, it can be seen that the SPR reflectivity curves move toward the largest angles of minimum reflectivity with the increase in d_{LiNbO_3} from 2 to 20 nm. This study demonstrates that SPR can be performed on a LiNbO$_3$ substrate with very good results compared to those obtained with glass substrates.

In order to understand the effect of the LiNbO$_3$ substrate on the biosensor performance, we have calculated the sensitivity as a function of d_{LiNbO_3} for two detection media of refractive indices 1.33 and 1.37. As shown in Fig. 4b, the sensitivity increases almost linearly when d_{LiNbO_3} increases from 135 deg/RIU to 280 deg/RIU. This gives a sensitivity improvement from 125 deg/RIU for BK7/Rh(10 nm)/
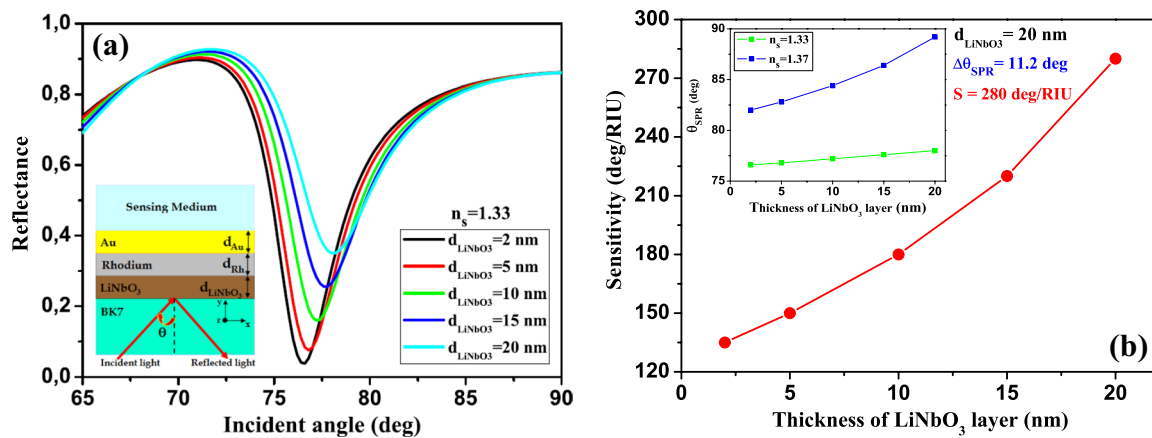
Fig. 4 **a** Reflectance intensity curves for different thicknesses of LiNbO$_3$ (d$_{LiNbO_3}$) and **b** Variation of sensitivity with thickness of LiNbO$_3$ layer (the inset shows the evolution of the resonance angle with thickness of LiNbO$_3$ film). For SPR nanostructure with 10 nm of Rh and 20 nm of Au

Table 2 Performance comparing of the nanostructure BK7/LiNbO$_3$/Rh(10nm)/Au(20nm) for different thicknesses of LiNbO$_3$ layer (d$_{LiNbO_3}$)

Thicknesses of LiNbO$_3$ film (nm)	Sensitivity (deg/RIU)	FWHM (deg)	FoM (RIU^{-1})
0	125	3.57	35.01
2	135	3.81	35.43
5	150	3.95	37.97
10	180	4.31	41.76
15	220	4.72	46.61
20	280	5.06	55.33

Fig. 5 Comparative analysis of different types of prisms in order to find maximum SPR angle for proposed sensor performance parameter analysis

Au(20 nm) to 280 deg/RIU for BK7/LiNbO$_3$(20 nm)/Rh(10 nm)/Au(20 nm).

This design of our proposed LiNbO$_3$ substrate SPR biosensor is approximately 2.44 times (124%) more sensitive than the glass substrate biosensor.

The thickness of the first LiNbO$_3$ layer (d$_{LiNbO_3}$) is a very important factor influencing the biosensor sensitivity (see Fig. 4b). Next, we consider the influence of d$_{LiNbO_3}$ on the FoM, as shown in Table 2. It shows the variation of FoM as a function of the thickness of the LiNbO$_3$ layer. From Table 2, it is shown that the FoM has a great improvement with increasing d$_{LiNbO_3}$. It is evident when the d$_{LiNbO_3}$ varies from 0 to 20 nm the FoM value increases from 35.01 RIU^{-1} to 55.33 RIU^{-1} is obtained for the SPR BK7/LiNbO$_3$/Rh(10 nm)/Au(20 nm) biosensor. In addition, the proposed biosensor shows a 58% (1.58 times) FoM improvement over the conventional BK7/Rh(10 nm)/Au(20 nm) sensor.

The optical properties of the materials constituting the prisms and their refractive index values have direct effects on the plasmonic response of the SPR biosensor. It is known that the prism amplifies the wave vector of the excitation wave and pro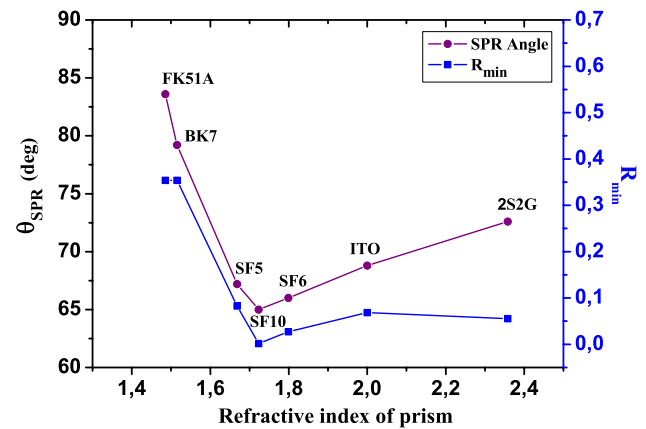vides a basis to make it coincide with the wave vector of the surface plasmon [47]. Figure 5 shows the SPR and minimum reflectance angle relative to the refractive index of the seven types of prism material at 633 nm. As shown in Fig. 5, the BK7 prism (n$_{BK7}$=1.5151) has the highest SPR angle with an appreciable R$_{min}$. These excellent SPR characteristics of the BK7 prism and its low refractive index are a choice for the ultimate design of our biosensor.

Previous studies on multilayer plasmonic biosensors with 2D nanomaterials have shown that the detection properties also depend on the number of monolayers of these 2D materials [28, 30, 48–50]. In this part of our study, we focus on the effect of the number of monolayers of 2D nanomaterials (Ti$_3$C$_2$T$_x$, BP and WS$_2$) on the detection performance of the BK7/LiNbO$_3$(10 nm)/Rh(10 nm)/Au(20 nm)/2D-nanomaterials biosensor.

First, we have studied the effect of the layers of Ti$_3$C$_2$T$_x$ MXene (L) on the reflectance intensity of the proposed

SPR biosensor shown in Fig. 6a, b for two different detection sensing of n_s=1.330 and n_s=1.335. The performance of the proposed SPR biosensor is greatly affected by the number of monolayer of $Ti_3C_2T_x$. Figure 6c shows the variation of θ_{SPR}, with respect to a different number L at λ = 633 nm. We notice a shift toward the higher θ_{SPR} values can be seen when L increases from L=0 to L=10, after θ_{SPR} decreases for L ≥ 10. This increase in the SPR resonance angle with the increase in the number of $Ti_3C_2T_x$ monolayer obtained on the reflectance curves (see Fig. 6a, b). The latter widen due to the increase in the loss of electronic energy (imaginary part of the refraction index increases) of the increased number of $Ti_3C_2T_x$ monolayers, as shown for graphene [51–53].

Figure 6d shows that there is a greater increase in sensitivity if the number of $Ti_3C_2T_x$ monolayers is varied from L=0 to L=6, and the greatest sensitivity S=240 deg/RIU can be obtained for L=6 compared to the nanostructure without $Ti_3C_2T_x$ (L=0) the sensitivity is S=128 deg/RIU. After that, the sensitivity starts to decrease for L > 6. It is concluded that the addition of 6 monolayers of $Ti_3C_2T_x$ the sensitivity is improved by 120%, this improvement is greater than that obtained by L. Wu et al [29]. However, when the

number of $Ti_3C_2T_x$ monolayers is increased the FoM starts to decrease from 41.76 RIU^{-1} to 17.43 RIU^{-1} due to the increased energy loss and the limitation of the angular range of the SPR resonance.

In a second phase, we have studied the influence of some BP (M) monolayers to improve the sensitivity of the proposed SPR biosensor BK7/LiNbO$_3$(10 nm)/Rh(10 nm)/Au(20 nm)/BP/sensing medium. Figure 7a, b shows the reflectance intensity spectra as a function of angle of incidence for the different number of BP (M) monolayers at two sensing media. From the figures, we can see that the minimum reflectance intensity corresponding to the SPR resonance angle is increased rapidly with the increase in BP monolayer from M=0 to M=5 due to increased absorption (due to its large real part of the refractive index n_{BP} = 3.5 + i0.01 at 633 nm). To understand the desired comparison, we first observe the addition effects of BP layers by plotting curves of the SPR resonance angle versus the number of BP monolayers for RI detection media 1.330 to 1.335 as shown in Fig. 7c. We notice a very good θ_{SPR} shift from 77.28 to 88.8 deg for n_s=1.330 and 77.72 to 89.8 deg for n_s=1.335 when M passes from 0 to 9 monolayers.
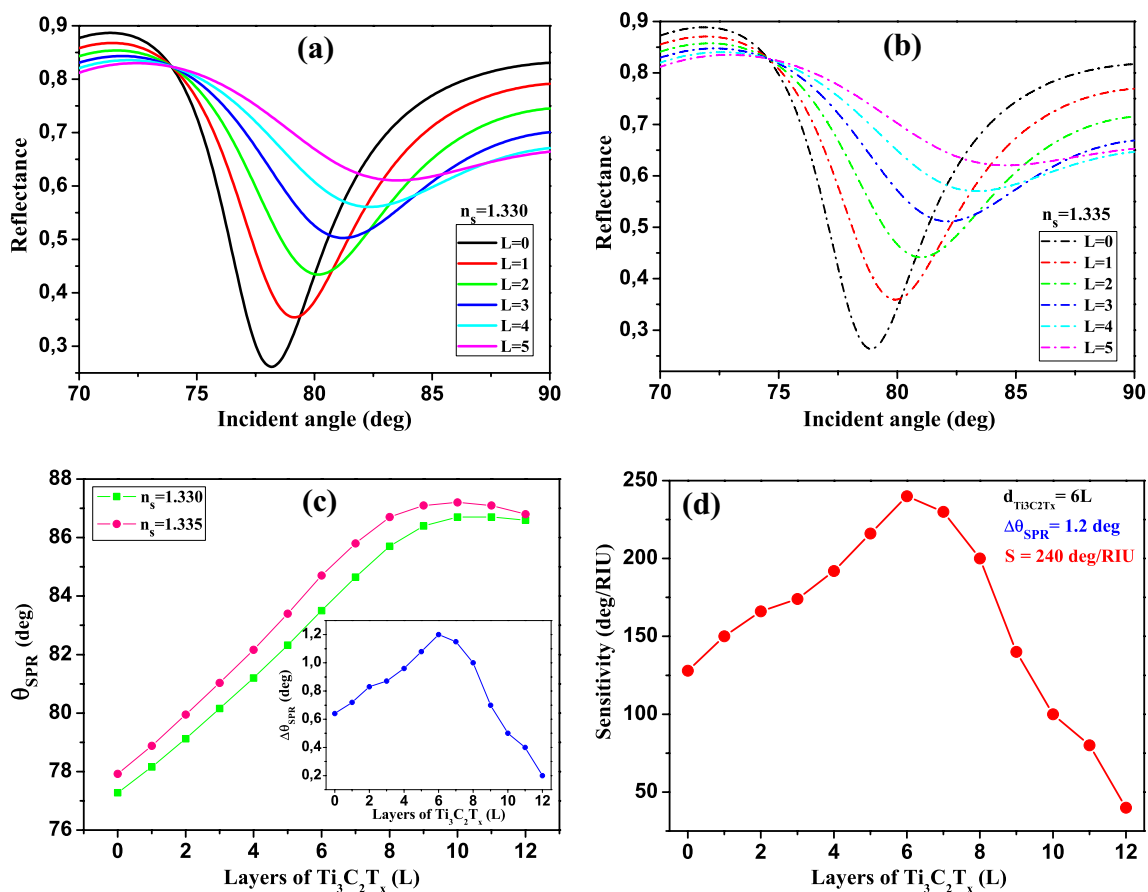

Fig. 6 a, b Reflectance intensity curves for different number of $Ti_3C_2T_x$ monolayer (L) [**a** for n_s=1.330, **b** for n_s=1.335]; **c** Evolution of the resonance angle and **d** Sensitivity as a function of the number of $Ti_3C_2T_x$ monolayer
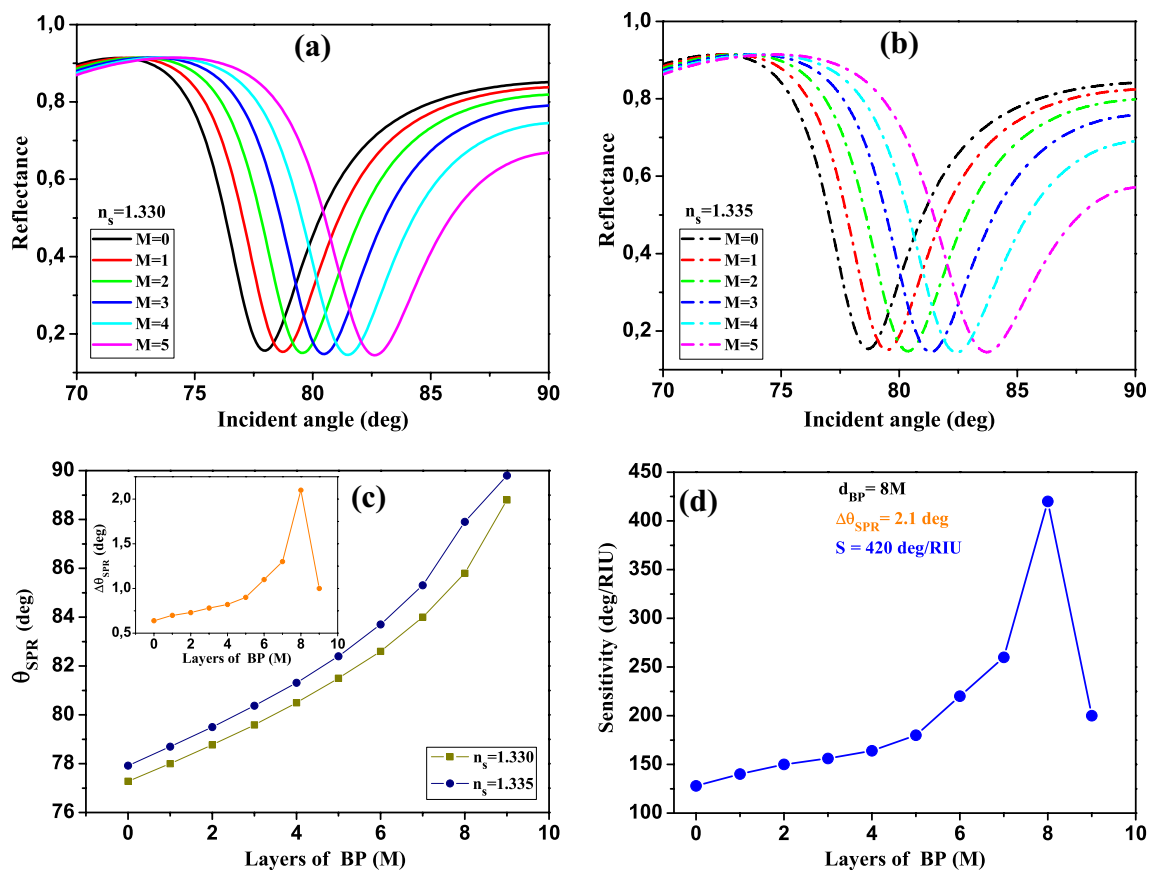
Fig. 7 **a**, **b** Evolution of reflectance with incident angle in different black phosphorus monolayer (M) [**a** for n_s=1.330, **b** for n_s=1.335]; **c** Evolution of the resonance angle and **d** variation of the Sensitivity with respect to the different number of black phosphorus monolayer (M)

Figure 7d shows the evolution of the sensitivity compared to the BP monolayer (M) for our proposed biosensor when the variation of the refractive index of the detection medium is Δn_s=0.005. According to the result, we have obtained that the sensitivity first increases to its maximum value S = 420 deg/RIU when the number of BP monolayer is 8 (M = 8), then starts to decrease when M > 8 (see Fig. 7d).

The result shows that the sensitivity is significantly improved by 210% (2.27 time) during application of 8 monolayers of BP compared to the biosensor at the sensitivity (S = 128 deg/RIU) of conventional structure without BP layer (BK7/LiNbO$_3$(10 nm)/Rh(10 nm)/Au(20 nm)).

Then, we have analyzed the effect of BP on the FoM in the first case means of conventional nanostructure (M = 0) the FoM=41.76 RIU^{-1}. As we can see, when you use different BP monolayers (M>0), the corresponding FoM is 31.8 RIU^{-1}. These results show that the FoM corresponding to maximum sensitivity is not necessarily maximum due to the increase in FWHM. This is due to the difference in optical conductivity of nanomaterials. The refractive index variation from three of BP monolayer is +3.18% [54].

In addition to the bimetallic multilayer SPR nanostructure with Ti$_3$C$_2$T$_x$ or BP, in this part we have optimized the effect of some monolayers of WS$_2$ (N) (transition metal dichalcogenides (TMDCs) element) to improve the detection performance properties of the proposed SPR biosensor BK7/LiNbO$_3$(10 nm)/Rh(10 nm)/Au(20 nm)/WS$_2$/Sensing medium.

Figure 8a, b shows the curves of reflectance intensity versus angle of incidence for a few WS$_2$ monolayers (from N=0 to N=4), when the refractive index of the sensing medium is increased from 1.330 to 1.335. The SPR curves have three very important characteristics due to its large real part of the refractive index: (i) The angular resonance shifts rapidly toward the larger θ_{SPR} (see Fig. 8c); (ii) as also shown in Fig. 8c, during the biodetection process, when the refractive index of the detection medium increases from 1.330 to 1.335 (Δn_s=0.005), a significant shift of $\Delta\theta_{SPR}$ occurs; and (iii) during this time, the full width at half height (FWHM) becomes wider due to the loss of electronic energy of the WS$_2$ layers [54].

The results obtained from optimization of the sensitivity as a function of the number of WS$_2$ monolayers presented in
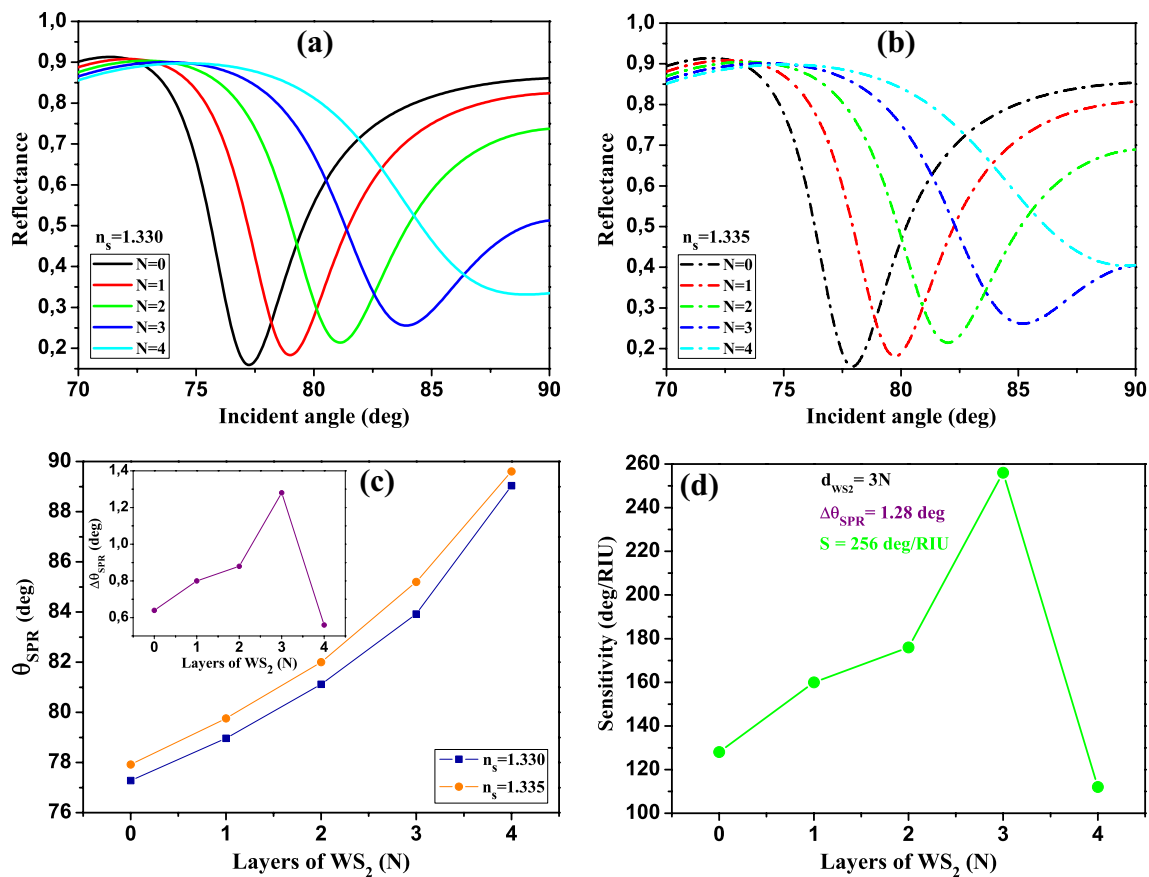
Figure 8 a, **b** Variation of the reflectance versus the incidence angle respect to the different number of WS$_2$ monolayer (N) [**a** for n$_s$ =1.330, **b** for n$_s$=1.335]; **c** evolution of the resonance angle versus the number N; and **d** variation of the sensitivity with respect to the different number of WS$_2$ monolayer (N)

Fig. 8d show that the highest sensitivity is $S = 256$ deg/RIU and the corresponding FoM is 30 RIU^{-1}, for the multilayer nanostructure at $N = 3$ monolayer of WS$_2$ very large to that obtained by the conventional configuration, of corresponding sensitivity of S=128 deg/RIU and FoM=41.76 RIU^{-1}. Figure 8d clearly shows that the WS$_2$ layer coating adapted to effectively improves the sensitivity of the proposed SPR biosensor. The sensitivity enhancement is 100% for N=3 monolayer of WS$_2$.

In contrast to sensitivity improvement, FoM is one of the important factors affecting the performance properties of biosensing. According to our results, the Ti$_3$C$_2$T$_x$-BP-WS$_2$ free nanostructure has the highest FoM. This is due to the fact that the energy loss induced by 2D nanomaterials will expand the FWHM. As we know, this phenomenon is also already reported in other work on 2D material-based SPR biosensors [28–31].

The results of monolayer number optimization of 2D nanomaterials show that sensitivity is desirable when there are many types of 2D nanomaterials added (see Fig. 1). The monolayer number optimization method is proposed

to quickly select the nanostructure for the ultra-sensitive biosensor. Figure 9a shows the sensitivity curves for Ti$_3$C$_2$ T$_x$, BP or WS$_2$-based biosensors. The optimized number of layers for each of the 2D nanomaterials is selected by the maximum value of sensitivity in these nanostructures as 6 monolayers of Ti$_3$C$_2$T$_x$ (S=240 deg/RIU), 8 monolayers of BP (S=420 deg/RIU), and 3 monolayers of WS$_2$ (S=256 deg/RIU) during the biosensing process, RI goes from 1.330 to 1.335.

As shown in Fig. 9b, the comparison of sensitivity improvements is 87.5%, 228.125% and 100% for the proposed BK7/LiNbO$_3$(10nm)/Rh(10nm)/Au(20nm) SPR biosensors, based on Ti$_3$C$_2$T$_x$, BP and WS$_2$, respectively.

Figure 10 discusses the nanoplasmonic response of the proposed SPR biosensor relative to the refractive index of the detection medium for different nanostructures. Figure 10a shows the reflectance curves of the BK7/LiNbO$_3$ (10nm)/Rh(10nm)/Au(20nm)/Ti$_3$C$_2$T$_x$(2L)/detection medium structure when the refractive index of the detection medium undergoes a slight change from 1.30 to 1.37 (Δn_s=0.01). In Fig. 10b, we have shown the relationship
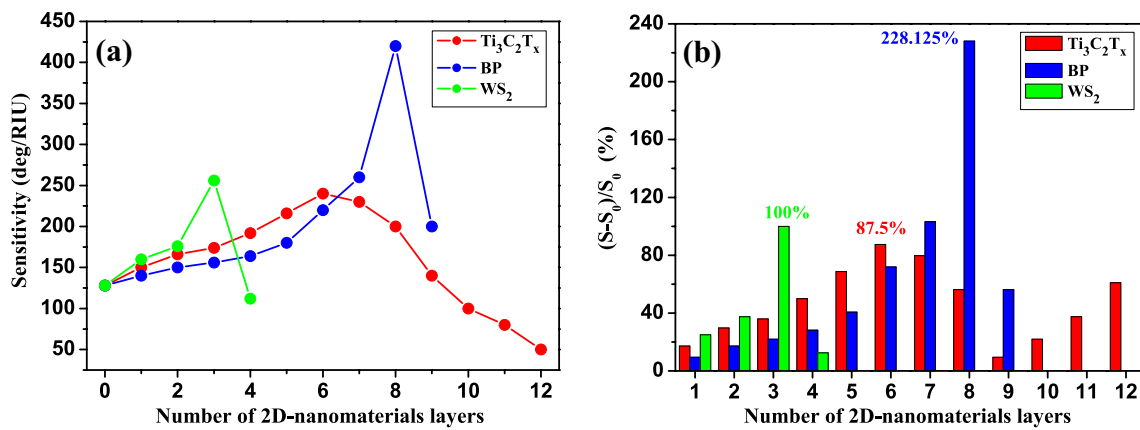
Fig. 9 **a** Comparative study of sensitivity and **b** shows the variation of the sensitivity enhancement with respect to the different number of $Ti_3C_2T_x$/BP/WS$_2$ monolayer when the variation of the refractive index of sensing medium is Δn_s=0.005
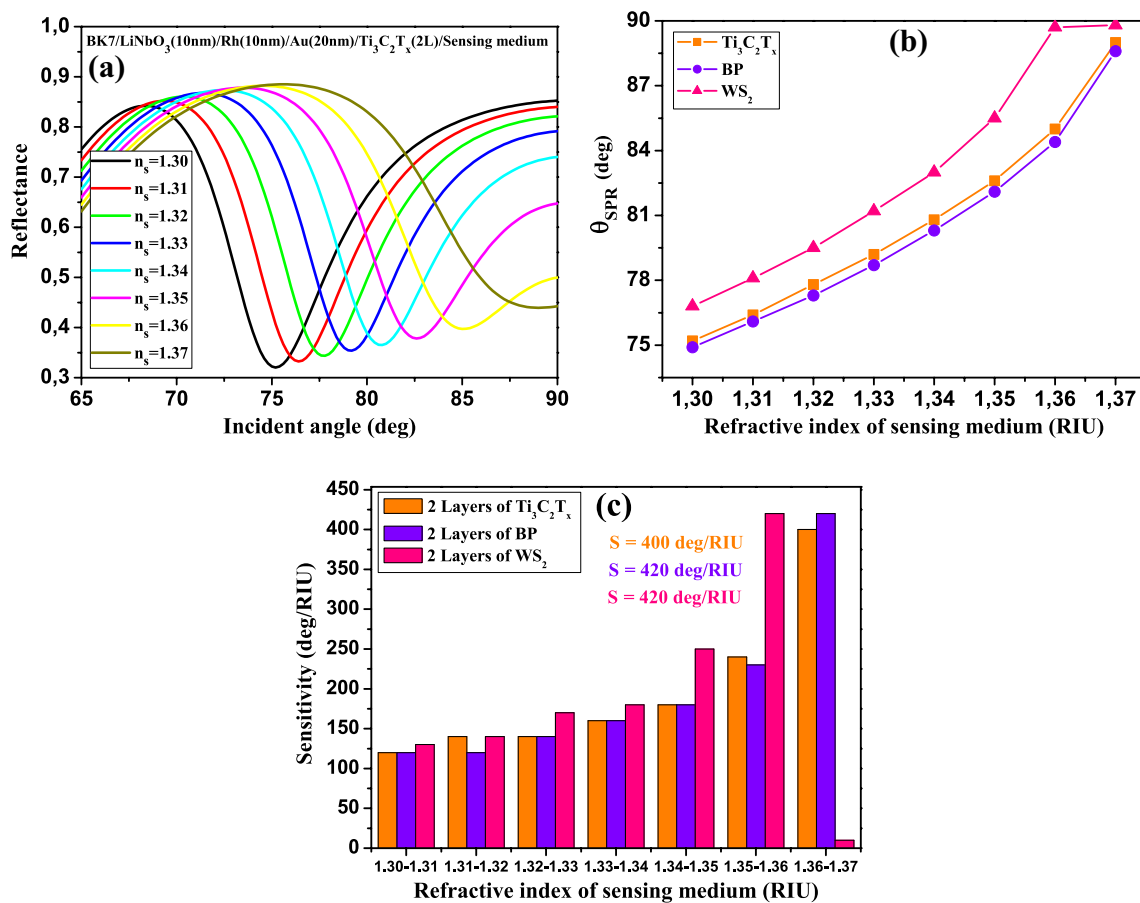

Fig. 10 **a** Variation of the reflectance with respect to the incident angle when the RI of sensing medium change from 1.30 to 1.37 (Δn_s =0.01) for the proposed biosensor with bilayer $Ti_3C_2T_x$ at λ=633 nm, **b** Evolution of the resonance angle with respect to the RI of sensing medium for different 2D-nanomaterials $Ti_3C_2T_x$/BP/WS$_2$ bilayer and **c** Variation of sensitivity with respect to the RI of sensing medium for the proposed biosensor with different 2D-nanomaterials $Ti_3C_2T_x$/BP/WS$_2$ bilayer

between the plasmon resonance angle and the variable of n_s, for the nanostructure with 2 monolayers of $Ti_3C_2T_x$, BP or WS$_2$, and it is clearly noticed that the resonance angle shifts toward the higher values when the refractive index of the detection medium varies from 1.30 to 1.37.

In the case of the nanostructure with WS_2, the resonance appears at a larger angle than in the nanostructure with $Ti_3C_2T_x$ or BP. This study clearly shows the quasi-linear response of the proposed SRP biosensor for different 2D detection nanomaterials, with the dynamic refractive index variation of n_s=1.30–1.37. Then, in Fig. 10c, we have shown the sensitivity to different refractive index variation of the detection medium of a pitch of Δn_s=0.01 using the results of Fig. 10b, and we can see that the sensitivity increases by 420 deg/RIU for WS_2 when ns is between 1.35 and 1.36, and by 400

deg/RIU and 420 deg/RIU for $Ti_3C_2T_x$ and BP, respectively, when ns is between 1.36 and 1.37.

Figure 11a–f shows the curves of electric field strengths versus normal distance from BK7 to the detection medium of the different studied mono- and bimetallic multilayer nanostructures for the proposed biosensors. The remarks made from Fig. 11a–c show that plasmon mode excitation depends on the coupling of the incident wave propagating in prism free space with the surface plasmon mode field at the interface between the metal film and the detection
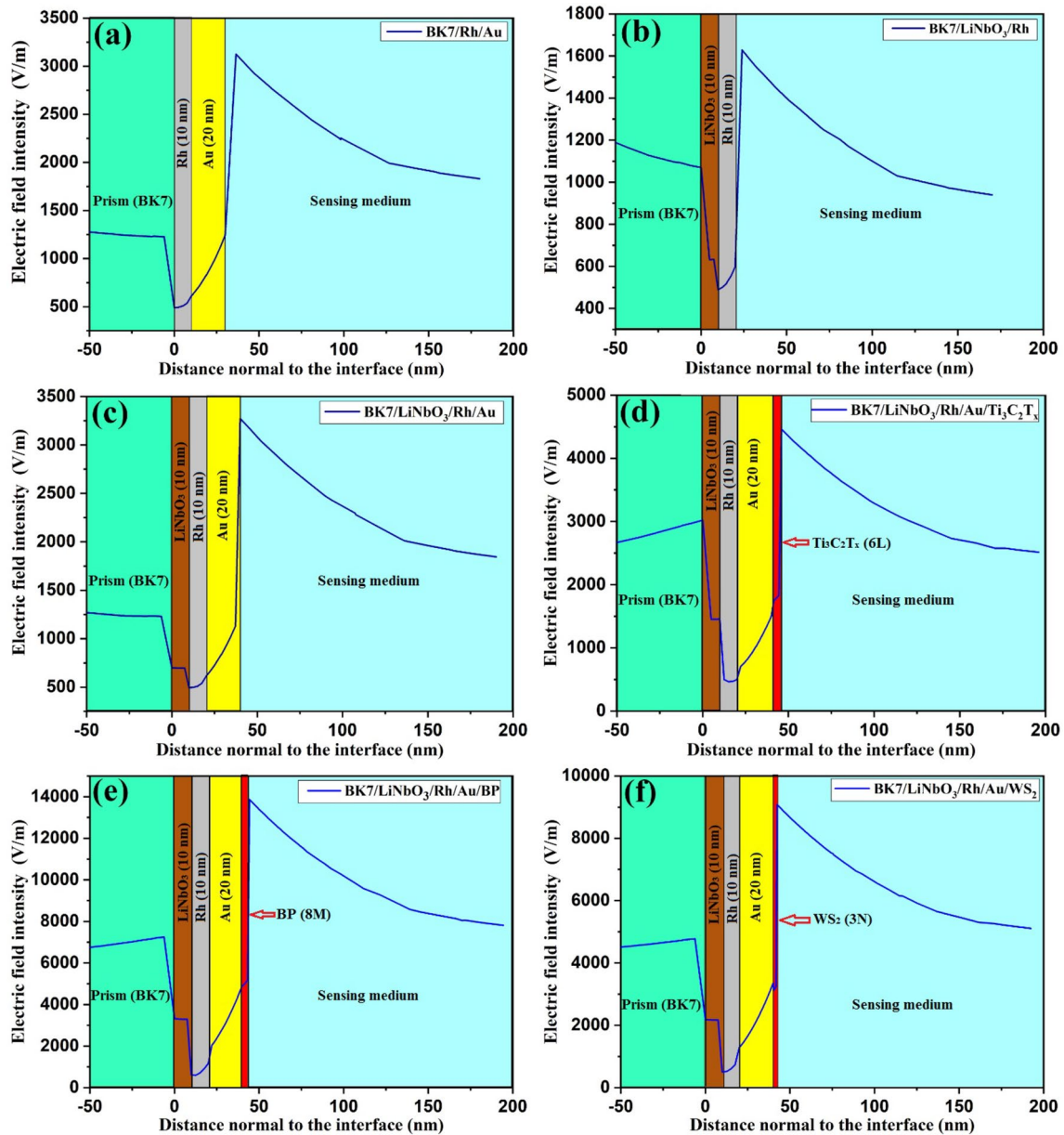

Fig. 11 Variation of electric field strength as a function of the normal prism distance at the interface of different nanostructures proposed for the RI of sensing medium n_s=1.330: **a** BK7/Rh/Au, **b** BK7/LiNbO$_3$/Rh, **c** BK7/LiNbO$_3$/Rh/Au, **d** BK7/LiNbO$_3$/Rh/Au/Ti$_3$C$_2$T$_x$, **e** BK7/LiNbO$_3$/Rh/Au/PB and **f** BK7/LiNbO$_3$/Rh/Au/WS$_2$

medium. It can be observed as shown in Fig. 11 that the electric field intensities in the prism part near the metal layer (50 nm in the vicinity of the metal layer) are different for the six nanometric configurations. In the nanostructure of the device studied in this manuscript (see Fig. 1), in the vicinity of the interfaces, we have an important variation of the refractive indices which causes a large variation of the electric field intensity. It can be noticed that the Au film progressively improves the field intensity that represents the surface plasmon excitation at this interface. Moreover, the decrease in the field intensity in the Rh film is governed by the large loss coefficient (imaginary part of the larger refractive index) [54–56]. In Fig. 11d–f, we observe that the highest field intensities come from the $Ti_3C_2T_x$, BP and WS_2 interface when the nanoplasmonic effect occurs near these interfaces, which improves the sensitivity of the proposed biosensors as shown in Figs. 9 and 10. It is obvious that the change of the nanoscale layer of the material deposited on the Au film will lead to a local change of the surface wave, which will further influence the electric field strength at this interface (see Fig. 11d, e). As shown in Fig. 11d–f, the electric field intensity reached the maximum at 4.5×10^3 V/m, 1.4×10^4 V/m and 9.1×10^3 V/m, which corresponds to the nanostructure with the $Ti_3C_2T_x$ layer (L=6), BP (M=8) and WS_2 (N=3), respectively. This shows an increase in field strength of 2.27×10^3 V/m compared to the nanostructure without these nanomaterials. At the level of the sensing medium, the intensity curve decreases exponentially with increasing distance from the interface.

4 Conclusion

In this work, we have theoretically studied a new SPR biosensor, using a hybrid bimetallic (Rh/Au) nanostructure coupled with a prism and a piezo-layer ($BK7/LiNbO_3$) at an excitation wavelength of 633 nm, to improve the biosensing accuracy and stability of our biosensor simultaneously. The proposed SPR device has increased sensitivity and FoM compared to the monometallic film-based SPR biosensor. For the RI detection medium ranging from 1.330-1.335, the obtained sensitivity and FoM values are 280 deg/RIU and 75.71 RIU^{-1}, respectively. Then we studied the influence of various 2D nanomaterials such as $Ti_3C_2T_x$ MXene, black Phosphorene and WS_2 are applied on the bimetallic biosensor surface to further enhance the sensitivity. We have shown that optimizing the number of monolayers of the coating of these three nanomaterials on the SPR biosensor surface can increase sensitivity due to its absorption. The values obtained are 240 deg/RIU for 6 monolayers of $Ti_3C_2T_x$, 420 deg/RIU for 8 monolayers of BP, and 256 deg/RIU for 3 monolayers of WS_2; the sensitivity improvements are 87.5%, 228.15%, and 100%, respectively, compared to the proposed SPR biosensor without nanomaterials on the surface. Due to its outstanding detection performance in the long range of RI 1.30 to 1.37 and its economical nanostructure and easy design, the proposed bimetal multilayer biosensor can be used effectively in bio- and chemical nanosensing technology and medical diagnostics.

References

1. S.J. Kim, H.J. Koh, C.E. Ren, O. Kwon, K. Maleski, S.Y. Cho, Y. Gogotsi, Metallic $Ti_3C_2T_x$ MXene gas sensors with ultrahigh signal-to-noise ratio. ACS nano **12**(2), 986–993 (2018)
2. J. Homola, Surface plasmon resonance sensors for detection of chemical and biological species. Chem. Rev. **108**, 462–493 (2008)
3. E. Wijaya, C. Lenaerts, S. Maricot, J. Hastanin, S. Habraken, J.P. Vilcot, R. Boukherroub, S. Szunerits, Surface plasmon resonance-based biosensors: From the development of different SPR structures to novel surface functionalization strategies. Curr. Opin. Solid State Mater. Sci. **15**, 208–224 (2011)
4. A.K. Sharma, Simulation and analysis of $Au-MgF_2$ structure in plasmonic sensor in near infrared spectral region. Optics Laser Technol. **101**, 491–498 (2018)
5. E. Kretschmann, H. Raether, Radiative decay of non radiative surface plasmons excited by light (Surface plasma wave excitation by light and decay into photons applied to non radiative modes). Z. Natur-forsch **23A**, 2135–2136 (1968)
6. A. Otto, Excitation of surface plasma waves in silver by the method of frustrated total reflection. Z. Physik **216**, 398–410 (1968)
7. L. Chen, J. Li, J. Liu, H. Yang, A Ag-Au bimetallic nanograting surface plasmon resonance sensor based on a prism structure. Opt. Commun. **461**, 125105 (2020)
8. A.K. Mishra, S.K. Mishra, R.K. Verma, Doped single-wall carbon nanotubes in propagating surface plasmon resonance based fiber optic refractive index sensing. Plasmonics **12**(6), 1657–1663 (2017)
9. C. Lin, S. Chen, Design of highly sensitive guided-wave surface plasmon resonance biosensor with deep dip using genetic algorithm. Opt. Commun. **445**, 155–160 (2019)
10. M. Setareh, H. Kaatuzian, Sensitivity enhancement of a surface plasmon resonance sensor using Blue Phosphorene/MoS_2 heterostructure and barium titanate. Superlattices Microstruct. **153**, 106867 (2021)
11. S. Franzen, Surface plasmon polaritons and screened plasma absorption in indium tin oxide compared to silver and gold. J. Phys. Chem. C **112**, 6027–6032 (2008)
12. J.H. Weaver, C.G. Olson, D.W. Lynch, Optical investigation of the electronic structure of bulk Rh and Ir. Phys. Rev. B **15**, 4115–4118 (1977)
13. S.K. Mishra, K.D. Malviya, A.K. Mishra, Highly sensitive bimetallic plasmonic sensing probe for aqueous samples. Opt. Quantum Electron. **52**, 284 (2020)
14. A.K. Mishra, S.K. Mishra, MgF_2 prism/rhodium/graphene: efficient refractive index sensing structure in optical domain. J. Phys. Condensed Matter **29**(14), 145001 (2017)
15. A.K. Mishra, S.K. Mishra, Gas sensing in Kretschmann configuration utilizing bi-metallic layer of Rhodium-Silver in visible region. Sensors and Actuators B: Chemical **237**, 969 (2016)
16. A. Ahmadivand, R. Sinha, S. Kaya, N. Pala, Rhodium plasmonics for deep-ultraviolet bio-chemical sensing. Plasmonics **11**(3), 839–849 (2016)

17. B. Meshginqalam, J. Barvestani, Aluminum and phosphorene based ultrasensitive SPR biosensor. Opt. Mater. **86**, 119–125 (2018)

18. J. Banerjee, M. Ray, Comparative performance evaluation of mono-metallic and bi-metallic plasmonic sensors using WS_2 and graphene with optical bio-sensing application. Sens. Actuators B Chem. **281**, 520–526 (2019)

19. A. Sinha, Z.H. Dhanjai, Y. Huang, X. Lu, J. Chen, R. Jain, MXene: an emerging material for sensing and biosensing. TrAC Trends Anal. Chem. **105**, 424–435 (2018)

20. M. Naguib, V.N. Mochalin, M.W. Barsoum, Y. Gogotsi, MXenes: a new family of two-dimensional materials. Adv. Mater. **26**, 992–1005 (2014)

21. Q. Ouyang, S. Zeng, J. Li, L. Hong, G. Xu, X.Q. Dinh, J. Qian, S. He, J. Qu, P. Coquet, K.T. Yong, Sensitivity enhancement of transition metal dichalcogenides/silicon nanostructure-based surface plasmon resonance biosensor. Sci. Rep. **6**, 28190 (2016)

22. H.O. Churchill, P. Jarilloherrero, Two-dimensional crystals: phosphorus joins the family. Nat. Nanotechnol. **9**(5), 330–331 (2014)

23. M.K. Singh, S. Pal, A. Verma, V. Mishra, Y.K. Prajapati, Sensitivity enhancement using anisotropic black phosphorus and antimonene in bi-metal layer-based surface plasmon resonance biosensor. Superlattices Microstruct. **156**, 106969 (2021)

24. R. Kumar, S. Pal, N. Pal, V. Mishra, Y.K. Prajapati, High-performance bimetallic surface plasmon resonance biochemical sensor using a black phosphorus MXene hybrid structure. Appl. Phys. A **127**(4), 1–12 (2021)

25. R. Kumar, S. Pal, Y.K. Prajapati, J.P. Saini, Sensitivity enhancement of MXene based SPR sensor using silicon: Theoretical analysis. Silicon, pp 1–8 (2020)

26. Y.K. Prajapati, A. Srivastava, Effect of BlueP/MoS_2 heterostructure and graphene layer on the performance parameter of SPR sensor: theoretical insight. Superlattices Microstruct **129**, 152–162 (2019)

27. S. Pal, A. Verma, Y.K. Prajapati, J.P. Saini, Sensitive detection using heterostructure of black phosphorus, transition metal dichalcogenides and MXene in SPR sensor. Appl. Phys. A **126**(10), 1–10 (2020)

28. X. Zhao, T. Huang, P.S. Ping, X. Wu, P. Huang, J. Pan, Z. Cheng, Sensitivity enhancement in surface plasmon resonance biochemical sensor based on transition metal dichalcogenides/graphene heterostructure. Sensors **18**(7), 2056 (2018)

29. L. Wu, Q. You, Y. Shan, S. Gan, Y. Zhao, X. Dai, Y. Xiang, Few-layer $Ti_3C_2T_x$ MXene: a promising surface plasmon resonance biosensing material to enhance the sensitivity. Sens. Actuators B Chem. **277**, 210–215 (2018)

30. L. Wu, J. Guo, Q. Wang, S. Lu, X. Dai, Y. Xiang, D. Fan, Sensitivity enhancement by using few-layer black phosphorus-graphene/TMDCs heterostructure in surface plasmon resonance biochemical sensor. Sens. Actuators B Chem. **249**, 542–548 (2017)

31. G. AlaguVibisha, J.K. Nayak, P. Maheswari, N. Priyadharsini, A. Nisha, Z. Jaroszewicz, K.B. Rajesh, R. Jha, Sensitivity enhancement of surface plasmon resonance sensor using hybrid configuration of 2D materials over bimetallic layer of Cu-Ni. Opt. Commun. **463**, 125337 (2020)

32. A. Srivastava, A. Verma, R. Das, Y.K. Prajapati, A theoretical approach to improve the performance of SPR biosensor using MXene and black phosphorus. Optik **203**, 163430 (2020)

33. S. Zeng, S. Hu, J. Xia, T. Anderson, X.Q. Dinh, X.M. Meng, P. Coquet, K.T. Yong, Graphene-MoS_2 hybrid nanostructures enhanced surface plasmon resonance biosensors. Sens. Actuators B **207**, 801–810 (2015)

34. U. Schlarb, K. Betzler, Refractive indices of lithium niobate as a function of wavelength and composition. J. Appl. Phys. **73**(7), 3472–3476 (1993)

35. D.E. Zelmon, D.L. Small, D. Jundt, Infrared corrected Sellmeier coefficients for congruently grown lithium niobate and 5mol.% magnesium oxide-doped lithium niobate. JOSA B **14**(12), 3319–3322 (1997)

36. J.H. Weaver, Optical properties of Rh, Pd, Ir, and Pt. Phys. Rev. B **11**(4), 1416 (1975)

37. B.D. Gupta, A.K. Sharma, Sensitivity evaluation of a multilayered surface plasmon resonance-based fiber optic sensor: A theoretical study. Sens. Actuators B Chem. **107**, 40–46 (2005)

38. A. Miranda, J. Halim, A. Lorke, M.W. Barsoum, Rendering $Ti_3C_2T_x$ (MXene) monolayers visible. Mater. Res. Lett. **5**(5), 322–328 (2016)

39. C. Shi, M. Beidaghi, M. Naguib, O. Mashtalir, Y. Gogotsi, S.J.L. Billinge, Structure of nanocrystalline Ti_3C_2 MXene using atomic pair distribution function. Phys. Rev. Lett. **112**, 125501 (2014)

40. Y. Jia, Z. Li, H. Wang, M. Saeed, H. Cai, Sensitivity enhancement of a surface plasmon resonance sensor with platinum diselenide. Sensors **20**(1), 131 (2020)

41. J.M. Jin, The Finite Element Method in Electromagnetics (Wiley-IEEE, 2014)

42. M. Besbes, J.P. Hugonin, P. Lalanne, S. van Haver, O.T.A. Janssen, A.M. Nugrowati, al., Numerical analysis of a slit-groove diffraction problem, J. Eur. Opt. Soc-Rapid Publ **2**(07022), 1–17 (2007)

43. P.K. Maharana, R. Jha, S. Palei, Sensitivity enhancement by air mediated graphene multilayer based surface plasmon resonance biosensor for near infrared. Sens. Actuators B Chemical **190**, 494–501 (2014)

44. B. Meshginqalam, J. Barvestani, Performance enhancement of SPR biosensor based on phosphorene and transition metal dichalcogenides for sensing DNA hybridization. IEEE Sens. J. **18**, 7537–7543 (2018)

45. A. Renaudin, V. Chabot, E. Grondin, V. Aimez, P.G. Charette, Integrated active mixing and biosensing using surface acoustic waves (SAW) and surface plasmon resonance (SPR) on a common substrate. Lab on a Chip **10**(1), 111–115 (2010)

46. D. Hao, M.G. Kenney, D.R. Cumming, Plasmonic gold nanodiscs using piezoelectric substrate birefringence for liquid sensing. Appl. Phys. Lett. **108**(25), 251601 (2016)

47. J.B. Maurya, Y.K. Prajapati, Influence of dielectric coating of metal layer in surface plasmon resonance sensor. Plasmonics **12**(4), 1121–1130 (2017)

48. M. El Barghouti, A. Akjouj, A. Mir, MoS_2 graphene hybrid nanostructures enhanced localized surface plasmon resonance biosensors. Opt. Laser Technol. **130**, 106306 (2020)

49. M. El Barghouti, A. Akjouj, A. Mir, Numerical analysis of MoS_2 on the LSPR in periodical nanostructure of Ag arrays/graphene for sensitive sensors. Int. J. Microwave Opt. Technol. **13**, 454–461 (2018)

50. M.H.H. Hasib, J.N. Nur, C. Rizal, K.N. Shushama, Improved transition metal dichalcogenides-based surface plasmon resonance biosensors. Condensed Matter **4**(2), 49 (2019)

51. M. El Barghouti, A. Akjouj, A. Mir, Effect of graphene layer on the localized surface plasmon resonance (LSPR) and the sensitivity in periodic nanostructure. Photon. Nanostruct. Fundam. Appl. **31**, 107–114 (2018)

52. M. El Barghouti, A. Akjouj, A. Mir, Reticular plasmon resonance detection properties of metal nanoparticles. Phys. E Low-dimensional Syst. Nanostructures **110**, 107–114 (2019)

53. M. El Barghouti, A. Akjouj, A. Mir, Design of silver nanoparticles with graphene coatings layers used for LSPR biosensor applications. Vacuum **180**, 109497 (2020)

54. Q. Peng, Z. Wang, B. Sa, B. Wu, Z. Sun, Electronic structures and enhanced optical properties of blue phosphorene/transition

metal dichalcogenides van der Waals heterostructures. Sci. Rep. **6**, 1–10 (2016)

55. A.M. Watson, X. Zhang, R. Alcaraz de La Osa, J.M. Sanz, F. Gonzalez, F. Moreno, G. Finkelstein, J. Liu, H.O. Everitt, Rhodium nanoparticles for ultraviolet plasmonics. Nano Lett. **15**(2), 1095–1100 (2015)

56. J.M. Sanz, D. Ortiz, R. Alcaraz de la Osa, J.M. Saiz, F. Gonzalez, A.S. Brown, M. Losurdo, H.O. Everitt, F. Moreno, UV plasmonic behavior of various metal nanoparticles in the near-and far-field regimes: geometry and substrate effects. J. Phys. Chem. C **117**(38), 19606–19615 (2013)

Publisher's Note Springer Nature remains neutral with regard to jurisdictional claims in published maps and institutional affiliations.

Authors and Affiliations

Mohamed El Barghouti[1] · **Abdellatif Akjouj[2]** · **Abdellah Mir[1]**

✉ Mohamed El Barghouti
  Mohamed.elbarghouti@gmail.com

1 Laboratory of Advanced Materials Studies and Applications (LEM2A), Physics Department, Faculty of Science, Moulay Ismail University of Meknes, B.P.11201 Zitoune, Meknes, Morocco

2 Univ. Lille, Institute of Electronics, Microelectronics and Nanotechnology, UMR CNRS 8520, FST, Villeneuve d'Ascq 59655, France